Sensors & Transducers, Vol. 185, Issue 2, February 2015, pp. 78-83

www.sensorsportal.com

Sensors & Transducers

http://www.sensorsportal.com

UV-VIS-NIR Communication with a-SiC:H Tandem Device

*** Vitor Silva, Paula Louro, Manuel A. Vieira, Isabel Rodrigues, Manuela Vieira**

Electronics Telecommunication and Computer Department ISEL – Instituto Superior de Engenharia de Lisboa, Lisboa, Portugal

CTS-UNINOVA, UNL - Universidade Nova de Lisboa, Caparica, Portugal

*E-mail: vsilva@deetc.isel.ipl.pt

Received: 14 November 2014 /Accepted: 15 January 2015 /Published: 28 February 2015

Abstract: Ultra-violet steady state illumination increases the spectral sensitivity of a pi'npin photodiode. Increased sensitivity in the range of 400-850 nm is experimentally demonstrated. The pi'npin photodiode can be illuminated on both back and front sides. Under front ultra-violet irradiation the gain is high for wavelengths in the 500-850 nm range and strongly quenches the 400-500 nm range. Under back ultra-violet irradiation the gain is high in the 400-500 nm range and strongly quenches for wavelengths in the 500-850 nm range. Using back or front illumination and the relative gain of each wavelength in the 400-850 nm range it is possible to select different wavelength channels. Results show that using different communication channels in the ultra-violet, visible and near infrared ranges the sensor exhibits a multiplexed output of all channels. By selectively illuminating the device with ultra-violet on the back or front sides of the device it enables the demultiplexing retrieval of all channels. *Copyright © 2015 IFSA Publishing, S. L.*

Keywords: Ultra-Violet, UV, Visible, Near Infrared, NIR, Visible Light Communication, SiC technology.

1. Introduction

Light-emitting Diode (LED) is a very effective lighting technology due to its high brightness, long life, energy efficiency, durability, affordable cost, optical spectrum and its color range for creative use. Their use as communication devices with a photo-diode as receptor, has been used for many years in hand held devices, to control televisions and other media equipment, and with higher rates, between computational devices [1]. This communication path has been used in the near infra-red (NIR) range, but due to the increasing LED lighting in homes and offices, the idea to use them for visible light communications (VLC) is present in many working groups. The Institute of Electrical and Electronics Engineers (IEEE) task group 7 has come up with the IEEE 802.15.7 VLC PHY/MAC standard proposal for the physical (PHY) and medium access control (MAC) for VLC communications [2]. The Internet use and its most popular protocols also have been studied for their performance over VLC [3]. Economic issues that will eventually guide the VLC outcome are also on the run [4]. The sensor presented in this paper, is based on amorphous silicon carbon technology (a-SiC:H) [5], it consists of a pi'npin structure. The front pi'n is thinner and has carbon a-SiC:H in the intrinsic layer while the back pin is based on a-Si:H. Two electrical optically transparent contacts interface the sensor at the front and back. Due to the asymmetric lengths of each pin structure and to their difference in materials, the sensor has

interesting properties, namely a light selective filter [6]. The sensor is capable of discriminating different wavelength signals and with convenient signal modulation has the capability of logic transformations (AND, OR, NOT and XOR) over the input signals [7], which may play an important function in specific VLC applications. A multiplexing / demultiplexing function has been identified using the sensor with 4 different channels allowing WDM applications [8]. The study of UV and IR response of the sensor is important for the possible use of these wavelengths as communication channels for out-of visible band information interchange [9]. In this paper, we demonstrate the use of near-UV steady state illumination to increase the spectral sensitivity of the a-SiC/Si pi'npin photodiode beyond the visible spectrum. Section 2 describes the pi'npin structure. Section 3 presents the theoretical optoelectronic model and linear state equations. Section 4 shows in graphical plots the experimental spectrum of the pi'npin photocurrent, and the photocurrent output for input signals in the visible and NIR spectrum ranges. Section 5 presents the results and their discussion. The conclusions and acknowledgement close the article.

2. Material and Methods

The sensor is composed by two stacked p-i-n structures (p(a-SiC:H)- i'(a-SiC:H)-n(a-SiC:H)-p(a-SiC:H)-i(a-Si:H)-n(a-Si:H)) sandwiched between two transparent contacts at each end. The thicknesses and optical gap of the i'- (200 nm; 2.1 eV) and i- (1000 nm; 1.8 eV) layers are optimized for light absorption in the blue and red ranges [10]. The working range of the sensor is in the visible spectrum, although light sources within the ultra-violet (350-400 nm) and near infra-red (700-880 nm) ranges are also used.

This 1 cm^2 structure can be seen in Fig. 1, where the wavelength arrows indicate the absorption depths during operation [11] and the digital light signals λ_V, λ_B, λ_G, λ_R, λ_{IR}, where the V index is in the UV range, R, G, B in the Visible and IR in the NIR range.

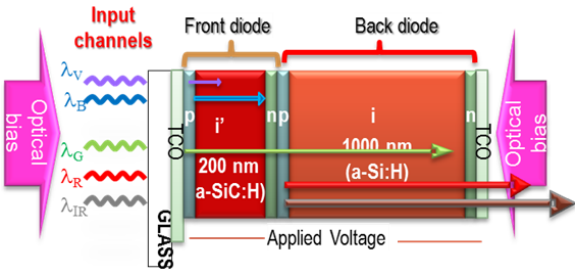

Fig. 1. Device structure and operation.

General purposes LEDs are used as light sources. These light sources are used as digital signals and background lighting. The signals are impinged on the front side of the sensor. The background lighting is either at the back or at the front side. The intensity of the signal sources is very low when compared to the background intensity. The LEDs that shine on the front surface, signal and background, are set at a distance of 3 cm, while the back led is almost touching the surface. Different wavelength signal sources are used: violet (400 nm), blue (470 nm), green (524 nm), red (626 nm) and infra-red (850 nm). For background lighting a 390 nm violet wavelength is applied. The signals are thus subject to constant background lighting and sampled at the midpoint of each bit. To change the background intensity different currents were used to drive the LED ($0 < I_{LED} < 30$ mA). The sensor working point is set at -8 V. The pi'npin device has a noise margin of 8 nA [12].

3. Theory

Based on the device configuration and experimental results an optoelectronic model was developed [13] and upgraded to include several inputs. The model is shown in Fig. 2. as an *ac* equivalent circuit.

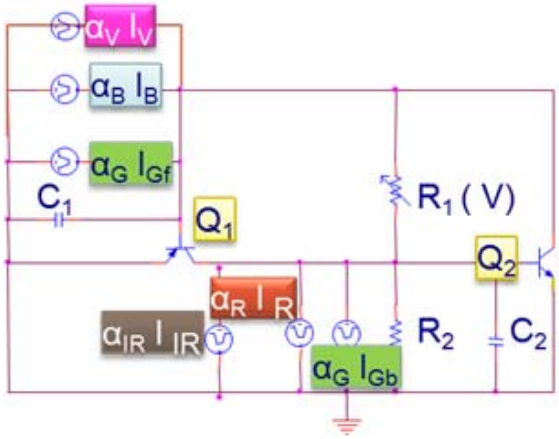

Fig. 2. ac equivalent circuit of the pi'npin photodiode.

The corresponding block diagram of the ac equivalent circuit of the pi'npin photodiode, and the linear state equations, are displayed in Fig. 3.

Input signals, $\lambda_{IR,R,G,B,V}$ model the input channels, and i(t) the output signal. The amplifying elements, α_1 and α_2 are linear combinations of the optical gains of each impinging channel, respectively into the front and back phototransistors, and provide gain ($\alpha>1$) or attenuation ($\alpha<1$) depending on the background effect.

The control matrix takes into account the enhancement or reduction of the channels, due to the steady state irradiation: front irradiation $\alpha_2 >> \alpha_1$ and back irradiation $\alpha_1 >> \alpha_2$. This affects the reverse photo capacitances, ($\alpha_{1,2}$ /$C_{1,2}$) that determines the influence of the system input on the state change (control matrix).

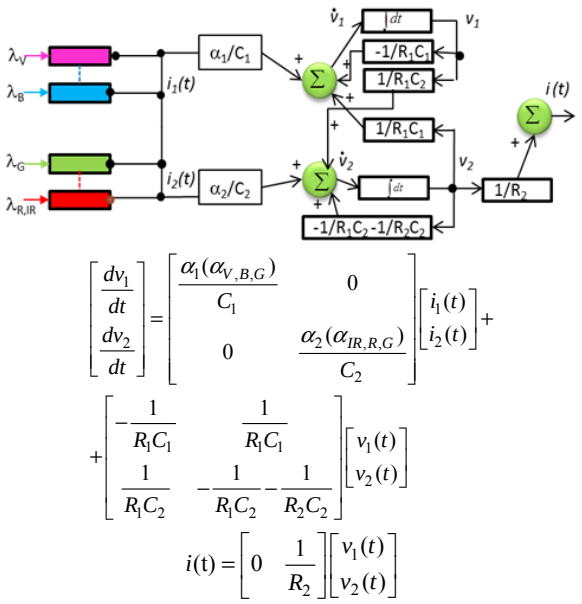

$$\begin{bmatrix} \frac{dv_1}{dt} \\ \frac{dv_2}{dt} \end{bmatrix} = \begin{bmatrix} \frac{\alpha_1(\alpha_{V,B,G})}{C_1} & 0 \\ 0 & \frac{\alpha_2(\alpha_{IR,R,G})}{C_2} \end{bmatrix} \begin{bmatrix} i_1(t) \\ i_2(t) \end{bmatrix} + \begin{bmatrix} -\frac{1}{R_1C_1} & \frac{1}{R_1C_1} \\ \frac{1}{R_1C_2} & -\frac{1}{R_1C_2} - \frac{1}{R_2C_2} \end{bmatrix} \begin{bmatrix} v_1(t) \\ v_2(t) \end{bmatrix}$$

$$i(t) = \begin{bmatrix} 0 & \frac{1}{R_2} \end{bmatrix} \begin{bmatrix} v_1(t) \\ v_2(t) \end{bmatrix}$$

Fig. 3. Block diagram and linear state equations.

A graphics user interface (GUI) computer program was designed and programmed with MATLAB® to ease the task of numerical simulation. This interface allows the selection of model parameters, and plots the photocurrent results of the simulated and experimental data. The simulation uses as a solver, one of two alternative algorithms: a one-step solver based on an explicit Runge-Kutta formula and an implementation of the trapezoidal rule using a "free" interpolant. An example is presented in Fig. 4.

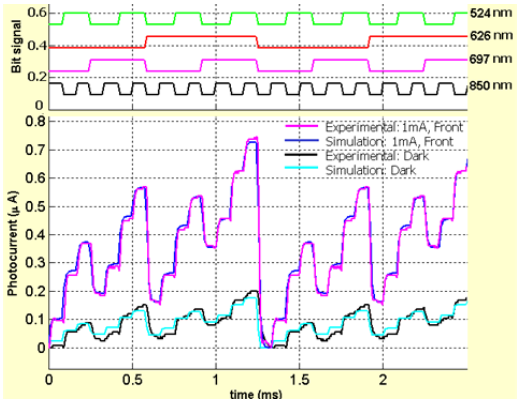

Fig. 4. Simulation example of the MUX signal with and without front λ=390 nm irradiation.

4. Experimental

4.1. Spectral Measurement

Using a monochromator with 1 mm slits and a chopper frequency of 3500 Hz, the spectrum measurements were made from 400 to 800 nm in 10 nm steps in three conditions: dark, front, and back. In the dark condition, the sensor is only subjected to the monochromator's light source.

These measurements (dark) are considered as a reference. The back or front conditions refer to a steady illumination of the back or front side of the sensor.

Several measurements were made with different background illumination intensities by applying currents in the 0.25 mA to 30 mA range, to the background LEDs with a wavelength of 400 nm. The results are presented in Fig. 5.

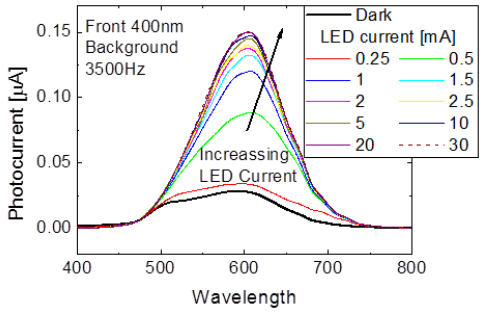

(a)

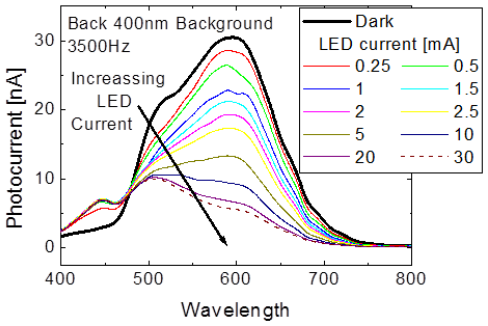

(b)

Fig. 5. Photocurrent spectrum with different background lighting intensities at the a) front and b) back side of the device.

Experimental output plotted in Fig. 5a, shows that with increasing front illumination (see arrow) by the violet LED there is an increase in the gain, from 470 to 750 nm. This increase is very effective, as a current of 0.5 mA is enough to produce an output 5 times higher than the dark level, which is represented in both Fig. 5a and Fig. 5b by a thick black curve. The influence of the back lighting in Fig. 5b with the same violet wavelength reduces the 470-750 nm bandwidth with increasing LED current. Photocurrent gain is defined as the ratio of the output in relation to the dark curve. The spectral gain for the different LED currents is shown in Fig. 6.

4.2. Visible / Infrared Tuning

Several monochromatic (850 nm, 697 nm, 626 nm, 524 nm, 470 nm, 400 nm) individually pulsed lights (input channels) at 12000 bps, and then

combined (MUX signal), illuminated the device while steady state 390 nm bias at different intensities ($0 < I_{LED} < 30$ mA) were superimposed separately, from either side of the sensor, and the photocurrent was measured.

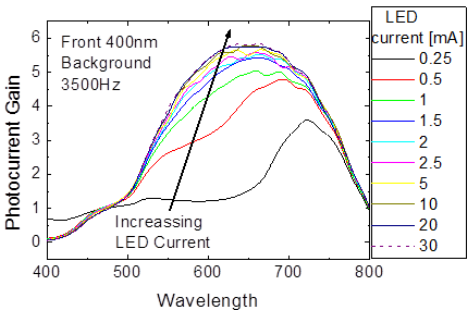

(a)

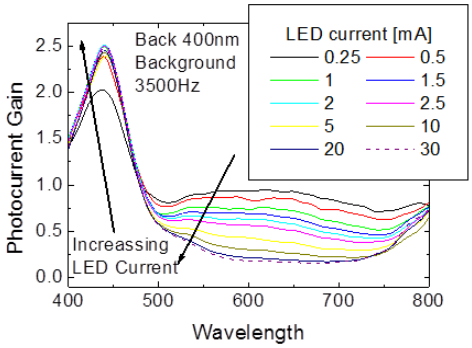

(b)

Fig. 6. Photocurrent gain with a) front and b) back illumination.

For each individual channel the photocurrent was normalized to its value without irradiation (dark), and the photocurrent gain determined. Fig. 7 displays the different gain as a function of the drive currents of the lighting LED under front and back irradiation.

To exemplify, in Fig. 8, the gain of the 850 nm input channel, under front irradiation at different intensities, is displayed.

4.3. Communication

The use of digital optical channels to communicate in the same medium is an application of this device [13-14]. Different wavelength channels transmit a digital signal and are multiplexed in the same medium. The light signal illuminates the pi'npin device and the signals are demultiplexed by applying ultra-violet illumination at the back and front sides [9]. An experiment using ultra-violet (400 nm), visible (470 nm, 524 nm, 626 nm) and near infra-red (700 nm) wavelengths is presented in Fig. 9. At the top of the figure, there are the signals used to drive the input channels, and are shown to guide the eyes into the on/off states.

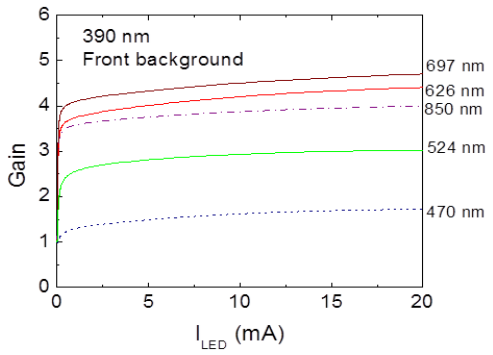

(a)

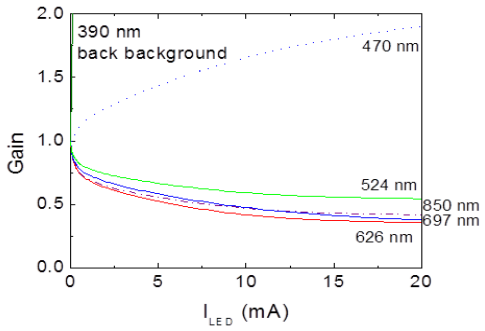

(b)

Fig. 7. a) Front and b) back optical gain at λ=390 nm irradiation and different input wavelengths.

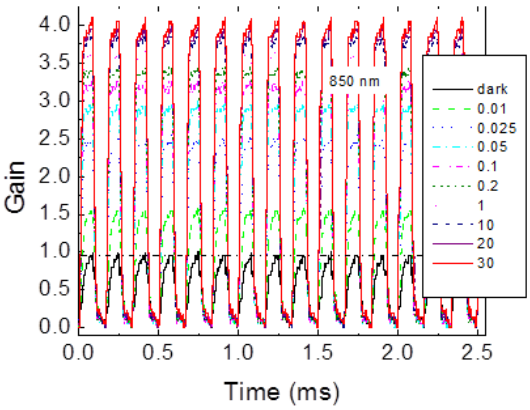

Fig. 8. Optical gain at 390 nm front irradiation with different intensities.

The output of the pi'npin device is presented in Fig. 9 without steady state ultra-violet radiation, called the Dark signal. All 32 possible combinations of the five input channels are visible, in an ascending binary count from 0 to 31. The same digital sequence is shown in Fig. 10 with the applied back and front steady state ultra-violet lighting.

The output signal in Fig. 10 is the result of the amplification or quenching according to the value of the individual gains of each wavelength when subjected to the back and front ultra-violet steady illumination.

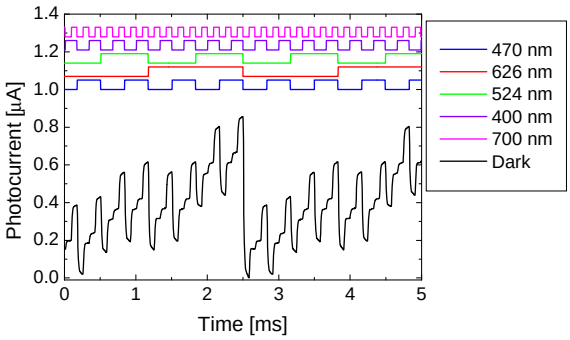

Fig. 9. Multiplexed signal with channels 400 nm, 470 nm, 524 nm, 626 nm, 700 nm, without ultra-violet steady state illumination.

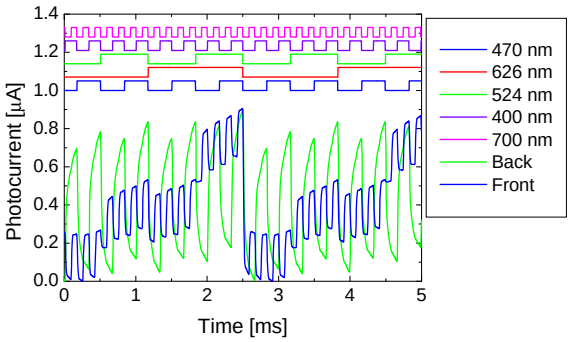

Fig. 10. Multiplexed signal with channels 400 nm, 470 nm, 524 nm, 626 nm, 700 nm, with back or front ultra-violet steady state illumination.

Fig. 11 shows the same digital light channel wavelengths of Fig. 9 but with a digital random sequence that contains all 32 possible combinations.

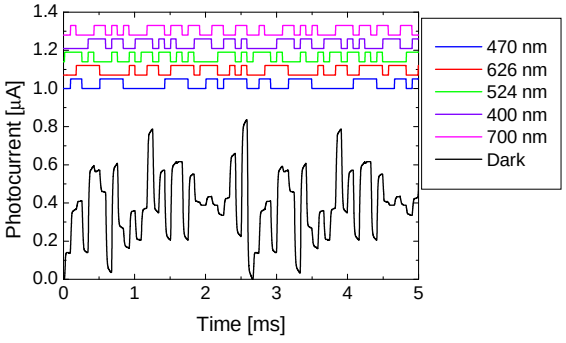

Fig. 11. Multiplexed output (Dark) with random data in channels 400 nm, 470 nm, 524 nm, 626 nm, 700 nm.

The random signal shown in Fig. 11 is the Dark signal without ultra-violet steady state illumination. At the top of the figure, there are the signals used to drive the input channels, and are shown to guide the eyes into the on/off states.

The retrieval of the original channels, shown in Fig. 12, is accomplished by illuminating the back and front sides of the device with a steady state ultra-violet illumination that will change the gain of each wavelength according to their relative position in the wavelength spectrum.

Displayed in Fig. 12 is the output due to the front and back ultra-violet steady state illumination. The correlation between these two signals identifies the original transmitted 5 bit code.

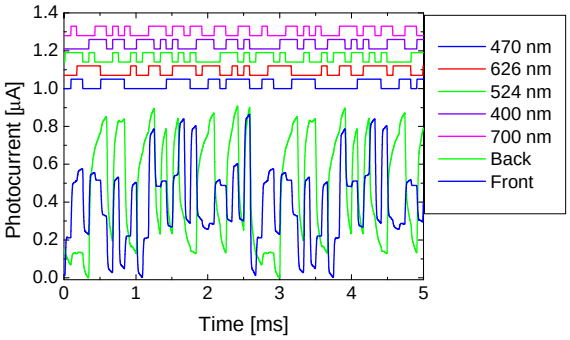

Fig. 12. Multiplexed random data channels 400 nm, 470 nm, 524 nm, 626 nm, 700 nm, with Back and Front output signals.

5. Results and Discussion

Results show, that background illumination of the front side, Fig 3a, reduces the 400-470 nm spectral range while it augments the 470-800 nm range. It acts as a selective filter for the long pass wavelengths. Background illumination of the back, Fig. 3b, enhances the 400-470 nm range and reduces the 470-800 nm wavelengths. It also acts as a selective filter but for the short pass wavelengths. This fundamental behaviour is the basis of the other possible functions that can be derived from it, besides a low pass or a long pass filter. Observing the gain values of the 850 nm IR wavelength presented in Fig. 7a and Fig. 7b, there is a significant difference that distinguishes the background lighting at the back or front side of the device by a wavelength of 390 nm. This allows for the recovery of a NIR channel by a UV background illumination which permits a communication channel outside the visible range. The individual magnitude of each input channel without background lighting (I_{LED}=0 in Fig. 7), was used to simulate the input channels. The results of the numerical simulation and the experimental results for the same sequence are presented in Fig. 4, and show that a good fitting between experimental and simulated results was achieved, showing the robustness of the proposed optoelectronic model.

The use of channels in the visible range of the spectrum, the Red (626 nm), Green (524 nm) and Blue (470 nm) wavelengths, with a ultra-violet (400 nm) and a near infra-red (700 nm) transmitted simultaneously with different digital data generate an electrical output on the pi'npin sensor, which is denoted as the Dark signal photocurrent show in the examples of Fig. 9 and Fig. 11. To aid the recovery

of the original channel data a steady state ultra-violet (390 nm) illumination floods the front and the back of the device each of them shown in Fig. 10 and Fig. 12. The Back signal shown on those figures follows mainly the 400 nm and 470 nm wavelengths data. The Front signal on the same figures follows mainly the 524 nm, 626 nm and 700 nm wavelengths data. In both Back and Front signal each wavelength has different gains according to the photocurrent gain of Fig. 6.

6. Conclusions

An increased sensitivity in a SiC pi'npin device in the VIS-NIR range under UV light was experimentally and theoretically demonstrated. Results show that under front 390 nm irradiation the sensor sensitivity was enhanced in the red/infrared ranges, leading to linearly profiled collection areas that allow the incoming wavelength recognition. An optoelectronic model was presented to explain the observed data, and allow decoding of multiplexed data in the visible/infrared range. The results of the numerical simulation are coherent with the experimental results for the same input sequence.

Several channels distributed along the ultra-violet, visible and near infra-red light wavelengths transmitted with different digital data can be received by a single pi'npin device and recovered by illuminating the back and the front side of the device with steady state ultra-violet light. Each wavelength responds to the back and front illumination with different gains. This method allows the recovery of the original channels.

Acknowledgment

This work was supported by FCT (CTS multi annual funding) through PIDDAC Program funds and PTDC/EEA-ELC/111854/2009 and PTDC/EEA-ELC/120539/2010.

References

[1]. T. Komiyama, K. Kobayashi, K. Watanabe, T. Ohkubo, Y. Kurihara, Study of visible light communication system using RGB LED lights, in *Proceedings of the IEEE SICE Annual Conference*, 2011, pp. 1926–1928.

[2]. S. Rajagopal, S. Lim, T. Bae, D. H. Kim, J. Son, I. S. Jang, D. Kim, D. W. Han, Y. Li, A. Yokoi, D. K. Jung, H. S. Shin, S. B. Park, K. W. Lee, S. A. Surra, F. Khan, T. G. Kang, E. T. Won, *IEEE 802.15 Wireless Personal Area Networks*, 2009, pp. 1–121.

[3]. V. V Mai, N. Tran, T. C. Thang, A. T. Pham, Performance analysis of TCP over visible light communication networks with ARQ-SR protocol, *Transactions on Emerging Telecommunications Technologies*, 2014, pp. 1–9.

[4]. H. Chowdhury, H. Bagheri, I. Ashraf, S. Tamoor-Ul-Hassan, M. Katz, Techno-Economic analysis of Visible Light Communications, in *Proceedings of the Tenth Int. Symp. Wirel. Commun. Syst. (ISWCS'13)*, Vol. 9, 2013, pp. 96–100.

[5]. G. De Cesare, F. Irrera, F. Lemmi, F. Palma, M. Tucci, a-Si:H/a-SiC:H Heterostructure for Bias-Controlled Photodetectors, *in Proceedings of the MRS Spring Meeting*, Vol. 336, 1994, pp. 885.

[6]. M. A. Vieira, Three Transducers for One Photodetector : essays for optical communications, PhD Thesis, *Universidade Nova,* Lisbon, 2012.

[7]. V. Silva, M. A. Vieira, M. Vieira, P. Louro, A. Fantoni, M. Barata, Logic functions based on optical bias controlled SiC tandem devices, *Phys. Status Solidi*, Vol. 11, No. 2, Feb. 2014, pp. 211–216.

[8]. M. A. Vieira, M. Vieira, P. Louro, A. Fantoni, A. Garção, Demux operation in tandem amorphous Si-C devices - A two stage active circuit, *i-ETCISEL Acad. J. Electron. Comput.*, Vol. 2, No. 1, 2013, pp. ID–13.

[9]. V. Silva, P. Louro, M. A. Vieira, I. Rodrigues, M. Vieira, Enhanced Sensitivity in the VIS-NIR Range Under UV Light in a-SiC Pinpin Devic, in *Proceedings of the 8th International Conference on Sensor Technologies and Applications (SENSORCOMM'14), Portugal,* Lisbon, 2014, pp. 17–20.

[10]. M. A. Vieira, M. Vieira, J. Costa, P. Louro, M. Fernandes, A. Fantoni, Double Pin Photodiodes with Two Optical Gate Connections for Light Triggering, *Sensors & Transducers*, Vol. 10, No. Special issue, 2011, pp. 96–120.

[11]. A. Fantoni, M. Vieira, R. Martins, Simulation of hydrogenated amorphous and microcrystalline silicon optoelectronic devices, *Math. Comput. Simul.*, Vol. 49, No. 4–5, Sep. 1999, pp. 381–401.

[12]. V. Silva, M. A. Vieira, P. Louro, M. Barata, M. Vieira, Simple and complex logical functions in a SiC tandem device, *Technological Innovation for Collective Awareness Systems*, 2014, pp. 592–601.

[13]. M. Vieira, P. Louro, M. Fernandes, M. A. Vieira, Q. Torre, M. Caparica, Three Transducers Embedded into One Single SiC Photodetector : LSP Direct Image Sensor, Optical Amplifier and Demux Device, in *Advances in Photodiodes (ed. Gian Franco Dalla Betta)*, Ch 19, 2011, pp. 403–426.

[14]. M. Vieira, P. Louro, M. A. Vieira, A. Fantoni, M. Fernandes, M. Barata, Optical Wavelength-division Multiplexing / Demultiplexing Devices, Revista Iberoamericana de Sensores, pp. 279–284.

[15]. P. Louro, V. Silva, I. Rodrigues, M. A. Vieira, M. Vieira, Home VLC using pinpin a-SiC:H multilayer devices, *MRS Proc.*, Vol. 1693, Jun. 2014, pp. 1-6.